Acta Polytechnica CTU Proceedings **48**:22–26, 2024
https://doi.org/10.14311/APP.2024.48.0022
© 2024 The Author(s). Licensed under a CC-BY 4.0 licence
Published by the Czech Technical University in Prague

A GEOMETRY PROJECTION METHOD FOR DESIGNING AND OPTIMIZING ADDITIVELY MANUFACTURED VARIABLE-STIFFNESS COMPOSITE LAMINATES

Yogesh Gandhi[a,*], Julián Norato[b], Ana Pavlovic[a], Giangiacomo Minak[a]

[a] *Alma Mater Studiorum – Università di Bologna, Department of Industrial Engineering, Via Fontanelle 40, Forlì-47121, Italy*

[b] *University of Connecticut, Department of Mechanical Engineering, 191 Auditorium Road, U-3139 Storrs, CT 06269, United States*

[*] corresponding author: yogesh.gandhi@unibo.it

Abstract. A method for designing laminates is presented using geometry projection to optimize the layout of additively manufactured variable-stiffness composite laminates. By considering fiber-reinforced bars as geometric primitives, the geometry projection methodology is extended to include optimizing regions with intersecting load paths. This is achieved by utilizing a dual representation of bars, which considers the geometric parameters and the element-wise density field representation. The dual representation enables the combining and overlapping of bars, resulting in a localized orthotropic material response at overlapping regions that mitigates the transverse compliant response of fiber-reinforced components. The proposed method's effectiveness is demonstrated through minimizing the compliance of the Messerschmitt-Bölkow-Blohm beam problem, a well-known benchmark problem in topology optimization.

Keywords: Topology optimization, geometry projection, continuous fiber-reinforced polymers, variable-stiffness laminates.

1. Introduction

Our study focuses on developing and optimizing variable-stiffness composite laminates (VSCLS) that can be produced using additive manufacturing. These VSCLs consist of layers with different orientations of fibers, which are customized to achieve specific mechanical properties, such as maximizing the stiffness-to-weight ratio. Designing VSCLs involves considering various factors, including fiber orientation, stacking order, and layer thickness. Unlike constant stiffness composites [1], optimizing VSCLs, as discussed elsewhere [2], is challenging due to the absence of analytical formulations. Therefore, designing VSCLs necessitate the use of discretization methods, such as the finite element method (FEM), to represent variations in material constituents. This leads to increased design variables, making the optimization process computationally intensive. As a result, computational design tools like topology optimization (TO) have become crucial for achieving the desired mechanical performance. These tools can also accommodate modifications resulting from advanced manufacturing processes [3], such as continuous fiber-fused filament fabrication (CF4).

Topology optimization (TO) is an iterative process for finding the optimal material distribution in a design domain, minimizing an objective function under constraints. Various methods include homogenization, solid isotropic material with penalization (SIMP) [4], level-set [5], evolutionary structural optimization, phase field, and feature mapping [6]. Details on these approaches have been reviewed elsewhere [7, 8]. Various techniques have also been advanced to determine the optimal distribution of fiber orientations within the design domain, as reviewed elsewhere [9].

In this paper, a geometry projection (GP) based [10] procedure is formulated to enable the design of VSCLs. While using fiber-reinforced bars (FRBs) as features, we modify the GP methodology in multiple ways. Initially, we leverage the dual nature of the geometry projection method to define overlapping FRBs in the design domain. These overlapping FRBs are then retained and modeled using composite laminate theory to calculate homogenized stiffness matrices, resulting in a local orthotropic material response. Additionally, forming overlapping FRBs in the design domain reduces the high strain energy density at intersecting load paths, which is further amiable for optimization. The component-wise GP formulation enables the seamless printing of VSCLs with the clear manifestation of overlapping components. Nonetheless, the proposed method to design VSCLs is limited to a single layer, which we call GP-AM.

2. Geometry projection formulation for variable-stiffness composite laminates

The GP procedure begins by mapping the design variables of the bar to a density field $\rho_{\mathrm{b}}(\boldsymbol{x};\boldsymbol{z}_{\mathrm{b}})$, where $\boldsymbol{x}$ represents any point in the design region. The dual geometric parameters/density representation can consider individual bars as high-level geometric objects or field variables in component densities.

The design in this work involves the combination of multiple FRBs. Each bar $b \in \mathcal{B}$, where $\mathcal{B}$ denotes the set of all bar indices, is represented as a rectangle with semicircular caps whose medial axis is a line segment, which occupies a region $\Omega_{\mathrm{b}} \in \mathbb{R}^2$. The medial axis is characterized by its two endpoints $(\boldsymbol{x}_{1\mathrm{b}}, \boldsymbol{x}_{2\mathrm{b}})$, and the offset distance corresponds to the radius r_{b} of the bar. A membership variable $\alpha_{\mathrm{b}} \in [0,1]$ is assigned to each bar and penalized similarly to density-based methods, allowing the optimizer to remove or include it in the design. The design variable vector $\boldsymbol{z}_{\mathrm{b}}$ for bar b is therefore expressed as:

$$\boldsymbol{z}_{\mathrm{b}} := (\boldsymbol{x}_{1\mathrm{b}}, \boldsymbol{x}_{2\mathrm{b}}, r_{\mathrm{b}}, \alpha_{\mathrm{b}})\,. \tag{1}$$

The projected density at a location $\boldsymbol{x}$ is determined by the intersection of a ball with a radius r and centered at $\boldsymbol{x}$ with Ω_{b}, i.e.:

$$\rho_{\mathrm{b}}(\boldsymbol{x};\boldsymbol{z}_{\mathrm{b}}) := \frac{|B^r_{\boldsymbol{x}} \cap \Omega_{\mathrm{b}}(\boldsymbol{z}_{\mathrm{b}})|}{|B^r_{\boldsymbol{x}}|}. \tag{2}$$

In 2D, under the assumption that r is significantly smaller than the dimensions of the bar, the intersection of $B^r_{\boldsymbol{x}}$ and $\partial\Omega_{\mathrm{b}}$ can be approximated as a line segment. As a result, the proportion of the projected density can be determined by calculating the proportion of the circular segment with a height of $h = r - \phi_{\mathrm{b}}$, where ϕ_{b} represents the signed distance from $\boldsymbol{x}$ to $\partial\Omega_{\mathrm{b}}$. The projected density for bar b is a uniquely determined function of ϕ_{b}, effectively functioning as a regularized Heaviside function:

$$\rho_{\mathrm{b}}(\boldsymbol{x};\boldsymbol{z}_{\mathrm{b}}) := \tilde{H}\left(\frac{\phi_{\mathrm{b}}(\boldsymbol{x};\boldsymbol{z}_{\mathrm{b}})}{r}\right). \tag{3}$$

The expression for $\tilde{H}$ is given.

$$\tilde{H}(x) = \begin{cases} 0, & \text{if } x \le -1 \\ 1 + \frac{1}{\pi}\left(x\sqrt{1-x^2} - \arccos x\right), & \text{if } |x| < 1 \\ 1, & \text{if } x \ge 1 \end{cases}$$

$$\frac{d\tilde{H}}{dx} = \begin{cases} 2\sqrt{1-x^2}/\pi, & \text{if } |x| < 1 \\ 0, & \text{otherwise}\,. \end{cases}$$

A penalized density is determined for each bar which is utilized to compute its elastic stiffness tensor. This is similar to the SIMP technique employed in density-based topology optimization [11]. The penalized density is expressed as:

$$\breve{\rho}_b^{eff}(\boldsymbol{x};\boldsymbol{z}_{\mathrm{b}}) := (\alpha_{\mathrm{b}}\rho_b(\boldsymbol{x};\boldsymbol{z}_{\mathrm{b}}))^{\mathrm{q}}\,, \tag{4}$$

where we recall q is the penalization factor.

2.1. Combining components

Eq. (2) pertains to the projection of a single bar. This study aims to focus on continuous fiber reinforcement, particularly in areas where multiple reinforcements overlap. This requires the material interpolation to accurately represent the stiffness that arises from overlapping bars. A straightforward approach is to compute the element's elasticity tensor as the sum of all elasticity tensors:

$$\boldsymbol{C}_{\mathrm{e}} = \boldsymbol{C}_{\mathrm{v}} + \sum_{\mathrm{b}=1}^{\mathrm{n_b}} \breve{\rho}^{\mathrm{eff}}_{\mathrm{be}}\left(\boldsymbol{C}_{\mathrm{b}} - \boldsymbol{C}_{\mathrm{v}}\right). \tag{5}$$

The elasticity tensor interpolation $\boldsymbol{C}_{\mathrm{e}}$ given by (5) can be used to interpolate between the solid material (bar material $\boldsymbol{C}_{\mathrm{b}}$) and void material $\boldsymbol{C}_{\mathrm{v}}$.

2.2. Elasticity tensor for overlapping components

The bar's material coordinate system (MCS), represented by $\{\hat{\boldsymbol{e}}_{1\mathrm{b}}, \hat{\boldsymbol{e}}_{2\mathrm{b}}, \hat{\boldsymbol{e}}_{3\mathrm{b}}\}$, is typically not the same as the laminate coordinate system (LCS), $\{\boldsymbol{e}_1, \boldsymbol{e}_2, \boldsymbol{e}_3\}$. We assume that the fiber reinforcement aligns with $\hat{\boldsymbol{e}}_{1\mathrm{b}}$, and we define $\hat{\boldsymbol{e}}_{2\mathrm{b}}$ so that it is orthogonal to $\hat{\boldsymbol{e}}_{1\mathrm{b}}$. Furthermore, we define $\boldsymbol{e}_3 = \hat{\boldsymbol{e}}_{1\mathrm{b}} \times \hat{\boldsymbol{e}}_{2\mathrm{b}}$ such that it corresponds to the global out-of-plane axis.

For plane stress of the laminate, the components of the elasticity tensor $\boldsymbol{C}_{\mathrm{b}}$ of bar b in LCS are given by

$$\boldsymbol{C}^{\mathrm{p}}_{\mathrm{b}} = \boldsymbol{T}_1^{\top}\hat{\boldsymbol{C}}^{\mathrm{p}}_{\mathrm{b}}\boldsymbol{T}_1 \qquad \text{and} \qquad \boldsymbol{C}^{\mathrm{s}}_{\mathrm{b}} = \boldsymbol{T}_2^{\top}\hat{\boldsymbol{C}}^{\mathrm{s}}_{\mathrm{b}}\boldsymbol{T}_2, \tag{6}$$

with

$$\boldsymbol{T}_1 = \begin{bmatrix} c^2 & s^2 & cs \\ s^2 & c^2 & -cs \\ -2cs & 2cs & c^2 - s^2 \end{bmatrix}, \; \boldsymbol{T}_2 = \begin{bmatrix} c & -s \\ s & c \end{bmatrix}, \tag{7}$$

where, c and s denote the cosine and sine of the angle θ respectively, where θ represents the angle between the axes $\hat{\boldsymbol{e}}_1$ and x. The 3×3 matrix $\hat{\boldsymbol{C}}^{\mathrm{p}}_{\mathrm{b}}$ establishes the relationship between the in-plane strains $\{\varepsilon_{\mathrm{x}}, \varepsilon_{\mathrm{y}}, \gamma_{\mathrm{xy}}\}$ and the stresses $\{\sigma_{\mathrm{x}}, \sigma_{\mathrm{y}}, \tau_{\mathrm{xy}}\}$ in LCS. Similarly, the 2×2 matrix $\hat{\boldsymbol{C}}^{\mathrm{s}}_{\mathrm{b}}$ governs the relationship between the out-of-plane shear strains $\{\gamma_{\mathrm{xz}}, \gamma_{\mathrm{yz}}\}$ and the stresses $\{\tau_{\mathrm{xz}}, \tau_{\mathrm{yz}}\}$ in LCS.

2.3. Elemental laminate elasticity matrix

For a laminate that is symmetrical with respect to the middle plane ($z = 0$) and consists of $2n_{\mathrm{b}}$ layers, the membrane-bending coupling matrix $\boldsymbol{D}_{\mathrm{md}}$ is equal to zero. We utilize the first shear deformation theory (FSDT) to analyze the mechanical behavior of VSCLs. In the FSDT, we relax Kirchhoff's theory by considering that the transverse normal no longer remains

Material	E_1	E_2	v_{12}	G_{12}	G_{13}	G_{23}
Carbon epoxy AS4/3501-6	113.6 GPa	9.650 GPa	0.334	6.0 GPa	6.0 GPa	3.1 GPa

Table 1. Material properties used for all the examples.

perpendicular to the mid-plane ($z = 0$) after deformation. This implies that the elastic displacement field within the laminate is expanded by as:

$$\begin{aligned} u(x,y,z) &= u_(x,y) + z\psi_{\mathrm{x}}(x,y) \\ v(x,y,z) &= v_0(x,y) + z\psi_{\mathrm{y}}(x,y) \\ w(x,y,z) &= w_0(x,y), \end{aligned} \tag{8}$$

where $u_0(x,y)$ and $v_0(x,y)$ represent in-plane displacements, while $w_0(x,y)$ represents the out-of-plane displacement. The subscript $(\cdot)_0$ indicates the displacement field of the reference plane.

Using four-node, bilinear, quadrilateral, and plane-stress elements, we construct element stiffness matrices based on the abovementioned assumptions. The stiffness matrix for the eth element can be represented as:

$$\begin{aligned} \boldsymbol{D}_{\mathrm{me}} &= \sum_{\mathrm{i}=1}^{\mathrm{n_b}} \left[h_{\mathrm{i}+1} - h_{\mathrm{i}}\right] \boldsymbol{C}^{\mathrm{p}}_{\mathrm{ei}}; \\ \boldsymbol{D}_{\mathrm{se}} &= \sum_{\mathrm{i}=1}^{\mathrm{n_b}} \left[h_{\mathrm{i}+1} - h_{\mathrm{i}}\right] \kappa \boldsymbol{C}^{\mathrm{s}}_{\mathrm{ei}}; \\ \boldsymbol{D}_{\mathrm{de}} &= \sum_{i=1}^{\mathrm{n_b}} \frac{1}{3} \left[h^3_{\mathrm{i}+1} - h^3_{\mathrm{i}}\right] \boldsymbol{C}^{\mathrm{p}}_{\mathrm{ei}}. \end{aligned} \tag{9}$$

Each bar is defined by the top and bottom planes $h_{\mathrm{i}+1}$ and h_{i}. The shear correction factor is $\kappa = 5/6$. Additionally, we assume that the layer thickness H is uniform, which means that $(h_{\mathrm{i}+1} - h_{\mathrm{i}}) = H$, and we also assume that the effect of stacking on the bending stiffness is disregarded, with $h_{\mathrm{b}} = 0$, leading to $(h^3_{\mathrm{b}+1} - h^3_{\mathrm{b}}) = H^3$ for all bars.

3. Optimization problem and sensitivity analysis

We address the minimization of compliance for a specified volume fraction limit. We formulate the optimization problem as follows:

$$\begin{aligned} &\min_{\{\boldsymbol{z}_{\mathrm{b}}\}} f := \log(c+1) \\ \text{subject to:} \quad & \\ & v \le \bar{v} \\ & \boldsymbol{K}\boldsymbol{U} = \boldsymbol{f} \\ & \underline{z}_{\mathrm{i}} \le z_{\mathrm{i}} \le \bar{z}_{\mathrm{i}}, i = 1, 2, \ldots, n_{\mathrm{z}}, \end{aligned} \tag{10}$$

where compliance, denoted by $c = \boldsymbol{U}^\top \boldsymbol{f}$, and $\boldsymbol{U}$ and $\boldsymbol{f}$ represent the global displacement and force vectors, respectively. The value $\bar{v}$ sets an upper limit on the volume fraction, while $\boldsymbol{K}$ represents the global stiffness matrix. The interval $[\underline{z}_{\mathrm{i}}, \bar{z}_{\mathrm{i}}]$ defines the lower and upper bounds on the i^{th} design variable.

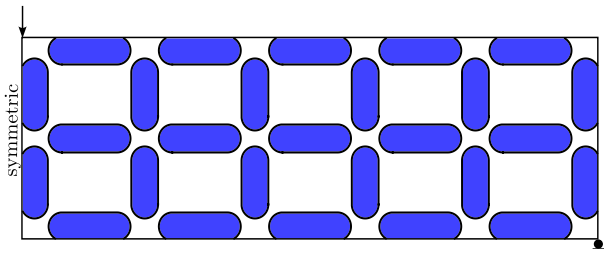

Figure 1. Design region, boundary conditions, and initial design for beam in 3−point in-plane bending.

The volume fraction, v, can be defined as

$$v^{(e)} := \frac{1}{\sum_{\mathrm{e}} \left|\Omega^{(\mathrm{e})}\right|} \left|\Omega^{(\mathrm{e})}\right| \sum_{\mathrm{b}} \rho^{\mathrm{eff}}_{\mathrm{be}}. \tag{11}$$

Finally, for the design-independent loading, the sensitivity of Eq. (10) and Eq. (11) is as follows:

$$\begin{aligned} \partial_{\mathrm{z_i}} c &= -\sum_{\mathrm{e}} \boldsymbol{u}^\top \left(\partial_{\mathrm{z_i}} \boldsymbol{K}^{(\mathrm{e})}\right) \boldsymbol{u} \\ \partial_{\mathrm{z_i}} v &= \frac{\sum_{\mathrm{e}} \left|\Omega^{(\mathrm{e})}\right| \partial_{\mathrm{z_i}} v^{(\mathrm{e})}}{\sum_{\mathrm{e}} \left|\Omega^{(\mathrm{e})}\right|}. \end{aligned} \tag{12}$$

The stiffness matrices design sensitivities $\boldsymbol{D}_{\mathrm{a}}$, where $\{a = m, d, s\}$ in Eq. (9) can be expressed in matrix form as follows:

$$\partial_{\mathrm{z_i}} \boldsymbol{D}_{\mathrm{e}} = \begin{bmatrix} \partial_{\mathrm{z_i}} \boldsymbol{D}_{\mathrm{me}} & \boldsymbol{0}_3 & \boldsymbol{0}_{3\times 2} \\ \boldsymbol{0}_3 & \partial_{\mathrm{z_i}} \boldsymbol{D}_{\mathrm{de}} & \boldsymbol{0}_{3\times 2} \\ \boldsymbol{0}_{2\times 3} & \boldsymbol{0}_{2\times 3} & \partial_{\mathrm{z_i}} \boldsymbol{D}_{\mathrm{se}} \end{bmatrix}. \tag{13}$$

For the matrix $\boldsymbol{0}_{\mathrm{n}}$, it's a zero matrix of size $n \times n$, and for $\boldsymbol{0}_{m\times n}$, it's a zero matrix of size $m \times n$. The chain rule is used to compute the design sensitivity of Eq. (13). This requires finding the derivative of the transformation in Eq. (6) and the penalized effective density. The computation of these derivatives is straightforward but has been left out for brevity. More detailed information can be found elsewhere [10].

4. Examples

We consider bars made of CFRP; fiber orientation is continuously aligned to the bar's axis. Table 1 lists unidirectional carbon-epoxy AS4/3501-6 material properties used for the bars.

The following settings are considered until mentioned otherwise. The method-of-moving-asymptotes (MMA) [12] optimizer is used for the optimization routine, with the default parameters described in here [13]. The void material assigned with a Young's modulus of $E^{\mathrm{void}} = 0.001$ GPa and a Poisson's ratio of $v^{\mathrm{void}} = 0.3$. In the initial design (see Figure 1), bars have a radius

Design	Combined density
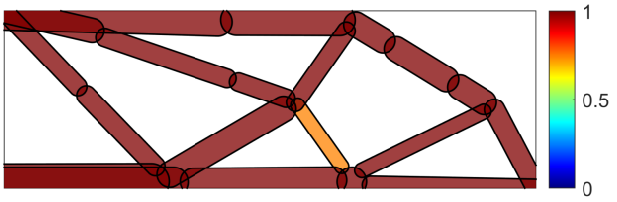	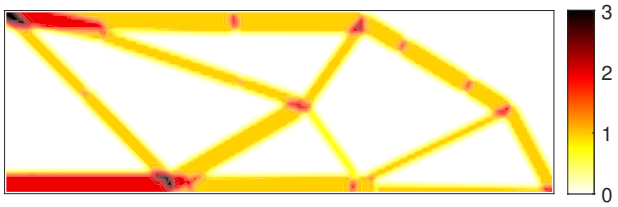

TABLE 2. Optimal designs and combined density for the MBB beam. The first column corresponds to the compliance value obtained by design, i.e., $c = 0.0905\,\mathrm{kN}\cdot\mathrm{mm}$. In the second column, transparency is used in the color of the bars for the GP-AM designs to help distinguish overlapping components. The color of the bars for the optimal designs in the last column corresponds to their penalized membership variable value $\alpha_{\mathrm{b}}^{\mathrm{q}}$, and the bars are plotted with transparency to facilitate the visualization of all bars.

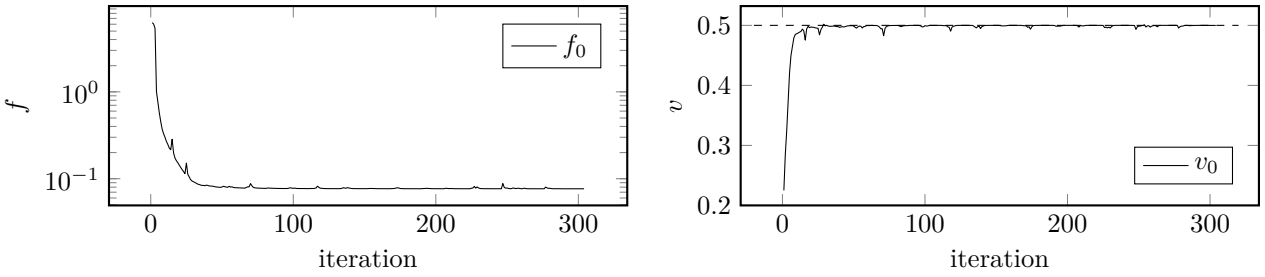

FIGURE 2. Objective (left) and volume constraint (right) history for the MBB beam design of Tab. 2 corresponding to the GP-AM design.

equal to the average of their upper and lower bounds during initialization. The sizing variable, α, is set to 0.5, and the move limit, m, is fixed and set to 0.02 throughout the optimization process.

The procedure of optimization entails three criteria for stopping. The first criterion is achieved when the 2-norm of the alteration in the vector of design variables is smaller than 0.002. The second criterion is attained when the KKT (Karush-Kuhn-Tucker) optimality condition norm is below 0.002. The third criterion is fulfilled when the modification in the objective function is less than 10^{-9}. The optimization process is stopped if any of these criteria are met.

4.1. BEAM IN 3-POINT BENDING

The example considers a $150\,\mathrm{mm} \times 50\,\mathrm{mm}$ simply supported beam in 3-point bending, as illustrated in Figure 1. The maximum volume fraction is 0.5. Because the problem is symmetrical, only the right side of the structure is modeled. Initially, the entire plate is designed with 27 bar, and the design variables are constrained within the following bounds.

$$\left\{ \begin{array}{c} (0,0) \\ 2 \\ 0 \end{array} \right\} \leq \left\{ \begin{array}{c} (\mathbf{x}_{b1}, \mathbf{x}_{b2}) \\ r_{\mathrm{b}} \\ \alpha_{\mathrm{b}} \end{array} \right\} \leq \left\{ \begin{array}{c} (150,50) \\ 5 \\ 1 \end{array} \right\} \quad (14)$$

In this situation, the highest bending stress occurs in the upper left corner where the load is applied, and the normal stresses cause tension on the bottom edge and compression on the top edge, with significant shear stresses near the neutral axis. Additionally, the optimal design for a single load application aligns bars' fiber reinforcement axis with the principal stress at each location [14].

In Table 2, it can be observed that there are horizontal bars at the top and bottom edges to represent the normal stress distribution, while inclined bars are used for the shear stress distribution. The overlapping bars contribute to a larger second-moment area of inertia, resulting in higher bending stiffness, which optimally supports the applied load. Furthermore, the method proposed in this study yields an optimal solution comparable to the findings of other density-based methods for the minimum compliance problem.

Figure 2 illustrates that the optimization process follows a usual convergence pattern for compliance; there is a significant decrease in the initial iterations, accompanied by minor adjustments to the design variables in the subsequent optimization iterations. Additionally, it displays a standard smooth convergence behavior.

5. CONCLUSIONS

The numerical experiment results demonstrate the effectiveness of the GP-AM in generating optimal solutions for the minimum compliance problem. From a manufacturing standpoint, the designs obtained with the proposed methods are amenable to manufacturing techniques for VSCL. Although not presented here for brevity, the proposed method produces good designs for several design regions, for example, problems: rectangular plate in pure torsion; cantilever beam under in- and out-of-plane bending; and square membrane in out-of-plane bending.

6. Acknowledgement

Financed by the European Union-NextGenerationEU (Grant No 2022NW83RE_002). The opinions expressed are those of the authors only and should not be considered representative of the European Union or the European Commission's official position. Neither the European Union nor the European Commission can be held responsible for them.

References

[1] H. Ghiasi, D. Pasini, L. Lessard. Optimum stacking sequence design of composite materials Part I: Constant stiffness design. *Composite Structures* **90**(1):1–11, 2009. https://doi.org/10.1016/j.compstruct.2009.01.006

[2] H. Ghiasi, K. Fayazbakhsh, D. Pasini, L. Lessard. Optimum stacking sequence design of composite materials Part II: Variable stiffness design. *Composite Structures* **93**(1):1–13, 2010. https://doi.org/10.1016/j.compstruct.2010.06.001

[3] J. Plocher, A. Panesar. Review on design and structural optimisation in additive manufacturing: Towards next-generation lightweight structures. *Materials & Design* **183**:108164, 2019. https://doi.org/10.1016/j.matdes.2019.108164

[4] G. I. N. Rozvany. A critical review of established methods of structural topology optimization. *Structural and Multidisciplinary Optimization* **37**:217–237, 2009. https://doi.org/10.1007/s00158-007-0217-0

[5] N. P. Van Dijk, K. Maute, M. Langelaar, F. Van Keulen. Level-set methods for structural topology optimization: A review. *Structural and Multidisciplinary Optimization* **48**:437–472, 2013. https://doi.org/10.1007/s00158-013-0912-y

[6] F. Wein, P. D. Dunning, J. A. Norato. A review on feature-mapping methods for structural optimization. *Structural and Multidisciplinary Optimization* **62**:1597–1638, 2020. https://doi.org/10.1007/s00158-020-02649-6

[7] O. Sigmund, K. Maute. Topology optimization approaches. *Structural and Multidisciplinary Optimization* **48**(6):1031–1055, 2013. https://doi.org/10.1007/s00158-013-0978-6

[8] J. D. Deaton, R. V. Grandhi. A survey of structural and multidisciplinary continuum topology optimization: Post 2000. *Structural and Multidisciplinary Optimization* **49**:1–38, 2014. https://doi.org/10.1007/s00158-013-0956-z

[9] Y. Gandhi, G. Minak. A review on topology optimization strategies for additively manufactured continuous fiber-reinforced composite structures. *Applied Sciences* **12**(21):11211, 2022. https://doi.org/10.3390/app122111211

[10] H. Smith, J. A. Norato. Topology optimization with discrete geometric components made of composite materials. *Computer Methods in Applied Mechanics and Engineering* **376**:113582, 2021. https://doi.org/10.1016/j.cma.2020.113582

[11] M. P. Bendsøe, O. Sigmund. Material interpolation schemes in topology optimization. *Archive of Applied Mechanics* **69**:635–654, 1999. https://doi.org/10.1007/s004190050248

[12] K. Svanberg. The method of moving asymptotes – a new method for structural optimization. *International Journal for Numerical Methods in Engineering* **24**(2):359–373, 1987. https://doi.org/10.1002/nme.1620240207

[13] K. Svanberg. MMA and GCMMA, versions September 2007. *Optimization and systems theory* **104**, 2007.

[14] P. Pedersen. Some general optimal design results using anisotropic, power law nonlinear elasticity. *Structural optimization* **15**:73–80, 1998. https://doi.org/10.1007/BF01278492